

Improved CTA Coronary Segmentation with a Volume-Specific Intensity Threshold

Muhammad Moazzam Jawaid¹(✉), Ronak Rajani², Panos Liatsis³,
Constantino Carlos Reyes-Aldasoro¹, and Greg Slabaugh¹

¹ City, University of London, London, UK
muhammad.jawaid.2@city.ac.uk

² Guys and St. Thomas Hospital, London, UK

³ The Petroleum Institute, Abu Dhabi, United Arab Emirates

Abstract. State-of-the-art CTA imaging equipment has increased clinician's ability to make non-invasive diagnoses of coronary heart disease; however, an effective interpretation of the cardiac CTA becomes cumbersome due to large amount of imaged data. Intensity based background suppression is often used to enhance the coronary vasculature but setting a fixed threshold to discriminate coronaries from fatty muscles could be misleading due to non-homogeneous response of contrast medium in CTA volumes. In this work, we propose a volume-specific model of the contrast medium in the coronary segmentation process to improve the segmentation accuracy. The influence of the contrast medium in a CTA volume was modelled by approximating the intensity histogram of the descending aorta with Gaussian approximation. It should be noted that a significant variation in Gaussian mean for 12 CTA volumes validates the need of volume-wise exclusive intensity threshold for accurate coronary segmentation. Moreover, the effectiveness of the adaptive intensity threshold is illustrated with the help of qualitative and quantitative results.

Keywords: Computed tomography angiography · Contrast medium · Curve evolution · Coronary segmentation

1 Introduction

Coronary heart disease (CHD) has become a major cause of death worldwide. According to recent statistics [13], CHD is responsible for approximately 73,000 deaths per year (an average of one death every seven minutes). Consequently, clinicians are interested in early detection of CHD to effectively predict and control future cardiac events. The limitations of conventional cardiac-angiography based diagnosis have driven intensive research for non-invasive diagnosis leading to highly sophisticated imaging procedures. The clinical use of computed tomography angiography (CTA) is a prominent example of non-invasive diagnosis, in which blood filled vasculature can be easily discriminated from the background based on high intensity. However, the high volume of imaging data demands

automatic segmentation of coronary vasculature as manual diagnosis becomes cumbersome and prone to inter-observer errors.

Apart from simple threshold and clustering techniques, the sophisticated algorithms employ partial differential equations (PDEs) to detect object boundaries, i.e. an initial guess is evolved under constraints to detect the object boundaries. Commonly used formulations include the *parametric snake model* and the *level set representation*. The parametric snake i.e. active contour model [9] leads to a fast and computationally efficient segmentation but shows greater sensitivity to the topological changes, whereas the level set representation [1, 14] provides inherent split and merge mechanisms to accurately detect complex structures at the cost of processing time. It should be noted that for both formulations, the evolution of the initially placed curve is regulated by an image based energy. Methods reported in [1, 9] approximate the image-based energy in terms of the intensity gradient strength (edge-map), whereas techniques proposed in [2, 19] employs regional intensity statistics for the energy approximation. The region-based methods show robust performance in general as the gradient strength often leads to over segmentation for weak edges. However, the conventional region-based methods fail to address the intensity inhomogeneity problem of medical images due to the underlying piecewise constant assumption. Consequently, Li *et al.* [11] and Lankton and Tannenbaum [10] proposed the use of localized statistics to regulate the curve growth in medical images for minimizing the impact of the intensity inhomogeneity.

In context of blood vessel segmentation in CTA, Harnandez *et al.* [6], Mohr *et al.* [12], Szymczak *et al.* [15], Wang and Liatsis [17] and Yang [18] reported successful segmentations; however, the impact of the externally injected contrast medium has been little employed in the coronary segmentation process. Isgum *et al.* [8] proposed an automated system for the coronary calcification detection, in which all the connected components of intensity value greater than 220 HU were interpreted as potential calcified plaques. Similarly, Hong *et al.* [7] proposed a fixed threshold of 350 HU for the segmentation of coronary calcified plaques in the contrast enhanced CTA.

In this work, we derive the estimate intensity threshold by investigating the impact of the contrast medium in the respective CTA volume to ensure the accuracy of segmentation. Followed with this introduction, we define the proposed coronary segmentation model in Sect. 2. Subsequently, comparative results are presented in Sect. 3, which is followed by the shortcomings and the conclusion.

2 Proposed Model

Based on the fact that externally injected contrast medium enhances the visual brightness of blood filled coronaries in CTA, we propose to adaptively model the contrast medium in the coronary segmentation process. The proposed method is classified as semi-automatic since it requires manual seed points to initialize the segmentation process. We start with the assumption that the coronary segmentation can be improved by suppressing the non-coronary structures using

intensity and shape constraints in a pre-processing step. However, the derivation of a generic intensity threshold across the dataset is challenging due to the non-homogeneous diffusion of the contrast medium in different CTA volumes. Consequently, the impact of the contrast agent is mathematically modelled in a first step to derive the volume-specific intensity range in Hounsfield units (HU) for respective CTA volumes. In the following step, we computed the voxel-wise vesselness measure using 3D Hessian matrix of the CTA volume to suppress the non-tubular voxels. In the final step, we applied the localized region based segmentation to extract coronary the tree from the pre-processed CTA volume. For the rest of the paper, let I denote a 3D CTA volume defined on the domain Ω and \mathbf{x}, \mathbf{y} denotes two independent spatial variables in the domain Ω . In addition, we employ a mask function $M(\mathbf{x}, \mathbf{y})$, which defines a neighbourhood of radius R_L centred at \mathbf{x} . Accordingly, the mask function $M(\mathbf{x}, \mathbf{y})$ will be 1 when a point \mathbf{y} lies within a neighbourhood region of \mathbf{x} , and 0 otherwise.

2.1 Contrast Medium Modelling

For enhanced visualization of the coronary vasculature, a contrast medium is often injected intravenously before the cardiac CTA exam. Consequently, the contrast affected blood appears brighter in the CTA volume which allows clinician to distinguish the coronary vasculature from the background as shown in Fig. 1a–b the diffusion of the contrast medium is non-homogeneous across patients as it depends upon several factors including the type and amount of contrast medium, the total scan time and the heart rate. This clinical fact leads to the assumption that despite of similar visual appearance of the blood filled coronaries, there exists a statistically significant difference in the blood intensity values for different CTA volumes. Consequently, the intensity based suppression of the non-coronary structures requires volume specific threshold values for optimal segmentation. Therefore, the use of a fixed threshold from the literature [7, 8] may result in erroneous segmentation. Based on the fact that the contrast affected blood flows into coronaries from the descending aorta, we therefore segmented the aorta in the first step to estimate the volume-specific HU intensity range. For aorta segmentation, we started with the background suppression in CTA using an intensity threshold of 100HU as shown in Fig. 1c. In the following step, we applied a circular Hough Transform [4] based shape analysis to segment the aorta from in the blood volume as shown in Fig. 1e. Iteratively, 2D segmentation is performed through axial slices until the circular aorta changes the shape which reflects the origin of coronary vasculature. Next, we computed the intensity histogram of the segmented aorta and the contrast medium response is modelled using Gaussian fitting. Figure 2a shows the Gaussian approximation for four CTA volumes where a significant variation in the mean values emphasize the need of an adaptive intensity threshold for accurate segmentation. It should be noted that the Gaussian mean represents the intensity for blood-filled aorta; however, the concentration of the contrast medium decreases as the blood flows towards distal segments of coronary tree. Moreover, the vessel narrowing towards the distal end points often result in the less diffusion and poor contrast. Thus,

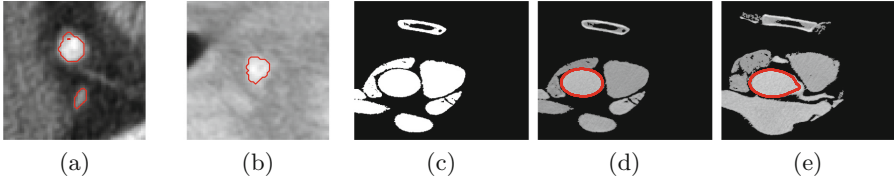


Fig. 1. Coronal appearance and aorta segmentation in axial slices. (a–b) Similar appearance for coronary in two CTA volumes. (c–d) Background suppression mask and the segmented aorta, (e) aorta shape change due to emerging coronary structure.

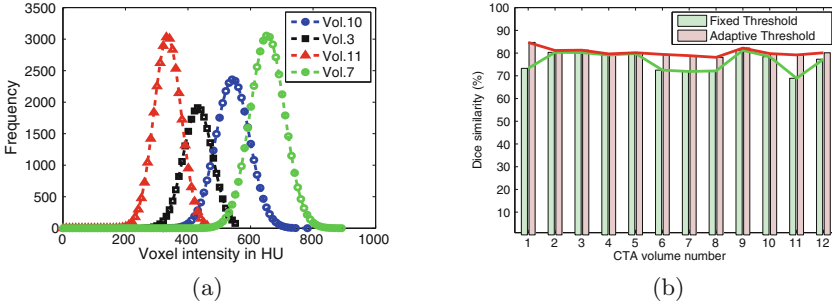


Fig. 2. Intensity approximation and mean accuracy for CTA volumes. (a) Shows the intensity distribution histogram for four CTA volumes in which a significant mean variation demonstrates the need of an adaptive intensity threshold. (b) Represents comparative segmentation accuracy for two intensity thresholds.

to take into account the intensity drop towards distal segments, we estimate the adaptive intensity range R_I for respective CTA volume I as expressed in Eq. 1.

$$R_I = \{\mu_I \pm 3\sigma_I\} \quad (1)$$

where μ_I and σ_I represent the aorta based mean HU and standard deviation for the respective CTA volume. For a quantitative comparison, the Gaussian distribution parameters and the derived intensity range for 12 clinical CTA volumes are presented in Table 1. It should be noted that the lower boundary of adaptive intensity range is meant for suppressing the non-coronary voxels and the upper boundary can be used to segment the calcified plaques (if any) in the arterial tree.

2.2 Enhancement of Tubular Structures

In this step, we employ shape information to effectively suppress the non-coronary voxels. Based on the fact that coronary vessels follow a tubular structure, we enhanced tubular voxels as proposed by Frangi *et al.* [5]. Accordingly, we obtained the 3D Hessian matrix of the CTA volume I in a first step to investigate the structural shape information. Next, we computed the eigenvalues from

Table 1. Volume-specific intensity (HU-range) for 12 CTA volumes.

CTA Vol	Mean HU	Std	Minimum HU	Maximum HU
01	942	62	756	1128
02	495	42	369	621
03	436	45	301	571
04	485	38	371	599
05	542	60	362	722
06	630	50	480	780
07	663	53	504	822
08	463	62	277	650
09	517	53	358	676
10	543	55	378	708
11	335	45	200	470
12	425	53	296	554

the 3D Hessian matrix to identify the geometric patterns and the voxel-wise vesselness is computed as follows:

$$V_o(\mathbf{x}) = \begin{cases} 0 & \text{if } \lambda_2 \text{ or } \lambda_3 > 0 \\ \left\{ 1 - \exp\left(-\frac{R_A^2}{2\alpha^2}\right) \exp\left(-\frac{R_B^2}{2\eta^2}\right) \left(1 - \exp\left(\frac{S^2}{-2\zeta^2}\right)\right) \right\} & \text{otherwise} \end{cases} \quad (2)$$

where $R_A = \frac{|\lambda_2|}{|\lambda_3|}$ discriminates plate-like structures from the cylindrical vessels, $R_B = \frac{|\lambda_1|}{\sqrt{|\lambda_2\lambda_3|}}$ differentiates blobs from other shapes and S serves as a penalty for the noise suppression. Moreover, the tuning parameters $\alpha = 0.6$, $\eta = 0.5$ and $\zeta = 220$ controls the overall vesselness measure. The response of the vesselness filter for 2D axial slices of CTA volume is shown in Fig. 3b, whereas the vesselness computed for the complete 3D CTA volume is presented in Fig. 3c. Figure 3b–c reflect that the tubular structures have been assigned high vesselness in comparison with the background; however, an inherent limitation of the multi-scale filter is misclassification of the edges, i.e. edges are often assigned comparatively high vesselness as well. This drawback is evident in Fig. 3c where it becomes extremely complex to identify the coronary vasculature. Consequently, the CTA

$$I(\mathbf{x}) = \begin{cases} I(\mathbf{x}) & \text{if } V_o(\mathbf{x}) > T_f \text{ and } I(\mathbf{x}) \in R_I \\ 0 & \text{otherwise} \end{cases} \quad (3)$$

volume I is filtered using intensity and vesselness constraints of Eq. 3 with T_f set equal to 10^{-3} .

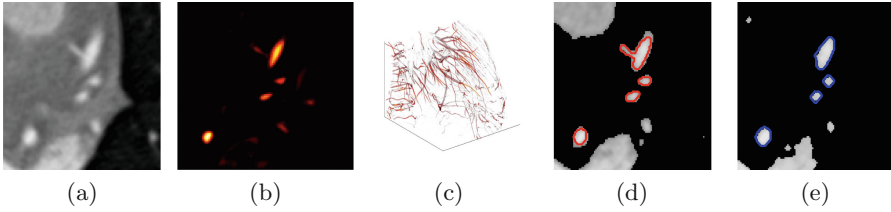


Fig. 3. Pre-processing for optimal segmentation. (a) Shows a 2D axial slice, (b–c) represent the 2D and 3D vesselness measure for CTA volume with prominent tubular structures and (d–e) show the intensity based background suppression using fixed and adaptive intensity threshold respectively. It can be observed that fixed threshold based segmentation (red) performs over segmentation due to leakage into nearby non-coronary structures, whereas (blue) contour represents the adaptive threshold segmentation. (Color figure online)

2.3 Coronary Tree Segmentation

Once the CTA volume is effectively filtered (as expressed in Eq. 3), the coronary tree is segmented using a 2D level set evolution based on the Chan-Vese [2] localized image energy. The segmentation process starts with the selection of the coronary seed points. To ensure that both coronary structures (left and right arteries) are segmented simultaneously, the coronary seed points are placed on an axial slice at the mid of the caudal-cranial axis. Next, the seed points are used to initialize a localized mask with a radius of 6 mm (i.e. maximum possible coronary diameter on an axial slice [3]). Subsequently, the initial mask evolves under the influence of image-based localized Chan-Vese energy to capture the true boundary of the coronary. Because of the 2D nature of the level set evolution, the evolved mask serves as an initialization to its adjacent axial slice on the caudal-cranial axis to capture the complete coronary tree. To define the mathematical model for level set coronary evolution, we start with the Chan-Vese segmentation in which two regions (the object and the background) are modelled with their mean intensity values as follows:

$$F(c_1, c_2, C) = \int_{in(C)} [I(\mathbf{x}) - c_1]^2 d\mathbf{x} + \int_{out(C)} [I(\mathbf{x}) - c_2]^2 d\mathbf{x} + \gamma length(C) \quad (4)$$

where C is the evolving curve, and c_1, c_2 represents the mean intensity value inside and outside the evolving curve respectively. For the level set formulation, the evolving curve C is embedded into a higher space using a signed distance function ϕ : such that $C = \{\mathbf{x} | \phi(\mathbf{x}) = 0\}$. The internal and external regions of the curve are defined using the Heaviside function (also termed as unit step function) $H\phi$, which is 1 when $\phi(\mathbf{x}) > 0$ and 0 when $\phi(\mathbf{x}) < 0$. Moreover, the evolving curve (zero level set) can be identified using derivative of Heaviside function i.e. the Dirac delta function δ which is 1 when $\phi(\mathbf{x}) = 0$ and 0 far from the interface. Accordingly, we formulate Eq. 4 using level set representation as expressed in Eq. 5. The first term of Eq. 5 is image-based curve driving energy

which minimizes the approximation error and the second term is the regularization term added to ensure the curve smoothness. For additional details and complete mathematical derivations, readers are referred to [2, 10].

$$\begin{aligned} \frac{\partial \phi}{\partial t}(\mathbf{x}) = & \delta \phi(\mathbf{x}) \int_{\Omega_{\mathbf{y}}} \phi(\mathbf{y}) M(\mathbf{x}, \mathbf{y}) \{ (I(\mathbf{y}) - c_1)^2 - (I(\mathbf{y}) - c_2)^2 \} d\mathbf{y} \\ & + \gamma \delta \phi(\mathbf{x}) \operatorname{div} \left\{ \frac{\nabla \phi(\mathbf{x})}{|\nabla \phi(\mathbf{x})|} \right\} \end{aligned} \quad (5)$$

where γ is the weight assigned to regularization term and c_1, c_2 represents the localized interior and exterior intensity mean values as expressed in 6. It should be noted that localization mask based statistics are used in the segmentation primarily due to the intensity inhomogeneity problem in medical data.

$$c_1 = \frac{\int_{\Omega_{\mathbf{y}}} M(\mathbf{x}, \mathbf{y}) I(\mathbf{y}) H \phi(\mathbf{y}) d\mathbf{y}}{\int_{\Omega_{\mathbf{y}}} M(\mathbf{x}, \mathbf{y}) H \phi(\mathbf{y}) d\mathbf{y}}, \quad c_2 = \frac{\int_{\Omega_{\mathbf{y}}} M(\mathbf{x}, \mathbf{y}) I(\mathbf{y}) (1 - H \phi(\mathbf{y})) d\mathbf{y}}{\int_{\Omega_{\mathbf{y}}} M(\mathbf{x}, \mathbf{y}) (1 - H \phi(\mathbf{y})) d\mathbf{y}} \quad (6)$$

2.4 Auto-correction Feature of the Mask

In general, the coronary tree comes out from the descending aorta and splits into branches along the caudal-cranial axis; hence all the segments are well captured in the level set based active contour evolution. However, due to the wide inter-patient variability and 2D axial slice based data acquisition in CTA, some distal branches emerge away from the main trajectory and become a part of the tree as slices are navigated. To address this issue, one possible solution is the 3D level set segmentation but it increases the computational load. In contrast, we introduced an auto-correction feature in the mask to capture the emerging peripheries during evolution. The proposed method reconstructs the mask in every iteration by scanning the neighbourhood of the trajectory on 2D axial slice. All the individual peripheries that satisfy the constraints (tubular shape and adaptive intensity) are captured as shown in Fig. 4c–d. This self-adjustment feature offers improved accuracy and the computational robustness, whereas the non-connected structures are automatically discarded using connected component analysis.

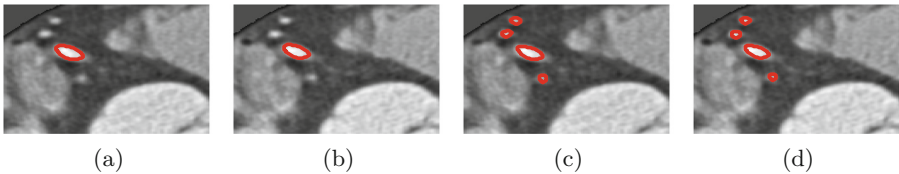


Fig. 4. Auto correction of mask to capture nearby emerging peripheries for CTA Volume (a–b), Emerging peripheries missed during evolution. (c–d), Emerging peripheries are captured for complete tree extraction.

3 Results

To demonstrate the effectiveness of the adaptive intensity modelling, the coronary segmentation was performed using two different intensity thresholds. The comparative results reveal that the use of fixed threshold i.e. 350 HU [7] leads to an erroneous coronary tree in terms of under/over segmentation, whereas the proposed adaptive threshold ensures accurate segmentation by employing the influence of contrast medium in the segmentation process. Moreover, the proposed segmentation shows a greater corroboration with the manual annotations in the cross sectional analysis as illustrated below.

3.1 CPR Based Analysis

Figure 5 shows the segmented right coronary artery (RCA) of CTA volume 1 using two different thresholds. Table 1 indicates that the strong concentration of the contrast medium requires a higher intensity threshold (756 HU) to minimize false positives. It can be observed from the figure that the volume-specific threshold precisely tracks the main progression of the RCA Fig. 5b from aorta to the distal segment with the minimal peripheries, whereas the use of a literature based [7] fixed threshold 350 HU results in numerous side branches for the RCA Fig. 5a. The efficacy of the adaptive intensity threshold is illustrated by constructing the curve planar reformatted (CPR) images along three different axes. CPR visualization from three different views helps to evaluate if there exist any intermediate peripheries for the segmented RCA. The centreline for the right coronary artery is obtained in the first step using sub-voxel skeletonization algorithm of [16]. In the subsequent step, we constructed the 2D CPR images from CTA volume as shown in Fig. 5c-e. It should be noted that distinct views along three different axes substantiate the fact that the right coronary artery is well segmented from aorta to the distal points using the adaptive intensity threshold. Moreover, it can be observed that the peripheries which appear to be a part of the coronary structure in Fig. 5a, are not coronaries indeed but the kissing vasculature in close proximity which were captured mistakenly by active contour during the evolution.

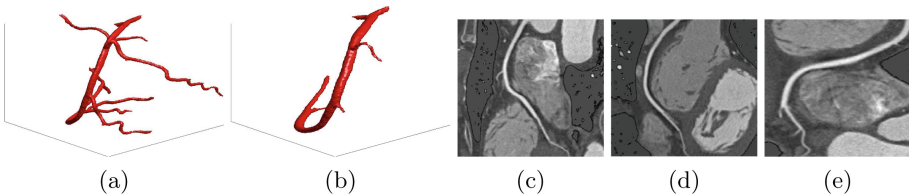


Fig. 5. Visualization of segmented RCA in CTA volume1, (a) RCA obtained using fixed intensity threshold of 350 HU, (b) RCA obtained using adaptive threshold. (c-e) Represent CPR image along three axes to confirm the efficacy of adaptive threshold.

3.2 Cross-Sectional Analysis

The efficacy of the adaptive intensity threshold is further illustrated by comparing the two segmentations in 3D space. Figure 6a–b shows a zoomed version of the segmented Left circumflex artery (LCX) branch of CTA volume 1 obtained using two thresholds. It should be noted that the adaptive threshold (756 HU) results in a smooth segmentation (see Fig. 6a), whereas the fixed threshold (350 HU) leads to over-segmentation in terms of disconnected expansion of the LCX. This is based on the fact that the high concentration of the contrast medium misleads the evolving curve to capture the nearby structures (see Fig. 6b). This over-segmentation is further unfolded using the orthogonal planar analysis as shown in Fig. 6c–d. The impact of the over-segmentation can be clearly observed by viewing the boundary points as the fixed threshold based segmentation shows incorrect expansion of the vessel in cross sectional planes in contrast to the response of adaptive threshold based segmentation.

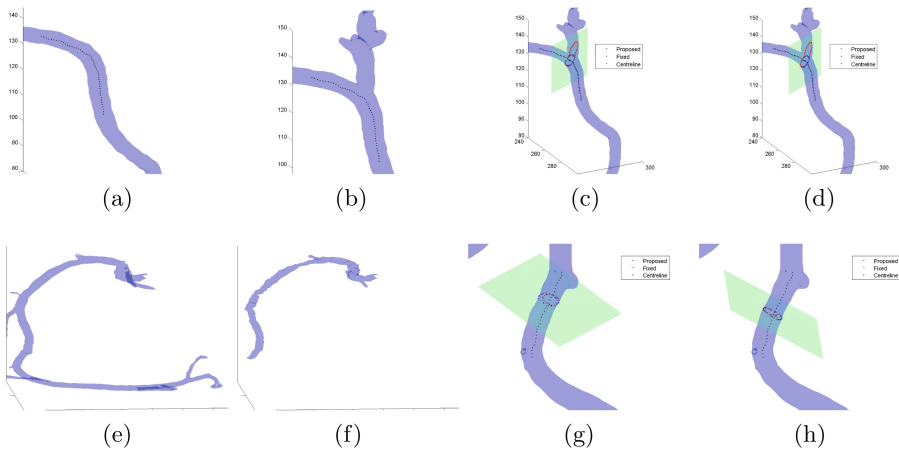


Fig. 6. Top. LCX branch of CTA volume 1. (a–b) LCX segmentation using adaptive (756 HU) and fixed (350 HU) threshold values respectively. (c–d) Illustrates the efficacy of adaptive threshold as planar boundary points show over-segmentation for fixed threshold. (Bottom) RCA branch of CTA volume 11. (e–f) RCA segmentation using adaptive (200 HU) and fixed (350 HU) threshold values respectively. (g–h) illustrates the efficacy of adaptive threshold as planar boundary points show under segmentation for fixed threshold. Red is the boundary for fixed threshold segmentation and green represents the response of adaptive threshold. (Color figure online)

Likewise, Fig. 6e–h present the case where the use of the fixed intensity threshold leads to an under-segmented tree because of low concentration of the contrast medium in CTA. The less concentration of contrast medium results in a lower intensity threshold in coronary segmentation, as Table 1 defines 200 HU for CTA volume 11. Figure 6e shows that adaptive threshold leads to detailed

coronary structure, whereas RCA obtained using a fixed intensity threshold of 350 HU shows under-segmentation as a significant portion towards distal RCA is missed (see. Fig. 6f). This under-segmentation becomes more evident in the planar analysis as the segmented lumen shrinks rapidly towards the distal segments. Figure 6g–h shows that the 350 HU based segmentation vanishes through the distal section of RCA in contrast to the response of adaptive threshold based segmentation.

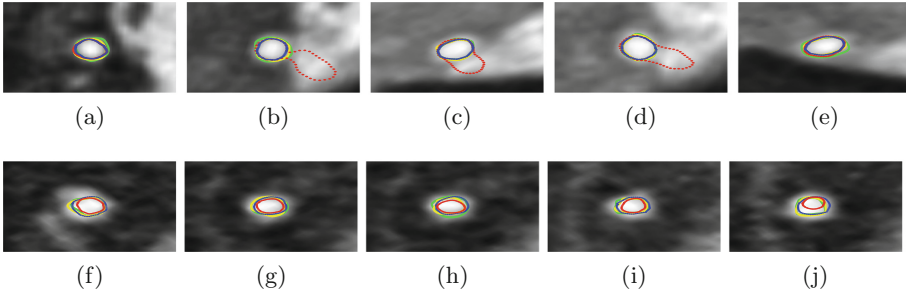


Fig. 7. Fixed and adaptive threshold based segmentation with respect to manual annotations. (Top) analysis for LCX of CTA volume 1 (bottom) analysis for RCA of CTA volume 11. Fixed threshold reflects over segmentation for CTA volume 1 and under segmentation for CTA volume 11. Red is the fixed threshold segmentation and green is the adaptive threshold result. Blue and yellow represents manual annotations. (Color figure online)

3.3 Validation Against Manual Annotations

The effectiveness of the volume-specific intensity threshold is also evaluated with respect to the manual annotations of two independent observers. Two well trained biomedical students were requested to perform the manual annotations of coronary lumen independently in our centre using interactive coronary analysis software. The lumen boundary obtained at the optimal coronary display settings ($L/W = 300/800$) are recorded for qualitative and quantitative evaluation of two segmentations. It can be observed from Fig. 7a–e) that the adaptive threshold leads to a good agreement with manual observers by suppressing the nearby vasculature, whereas the fixed threshold based segmentation captures the adjacent non-coronary structures that results in increased false positives. Likewise, Fig. 7f–j) show the response of two segmentations for RCA of CTA volume 11. It should be noted that the adaptive threshold leads to a true segmentation by allowing expansion towards low intensity voxels, whereas the fixed intensity threshold favours high intensity voxels resulting in under-segmentation. To demonstrate the quantitative efficiency of the adaptive intensity threshold, we computed the segment-wise accuracy with respect to the manual annotation

using three metrics i.e. sensitivity, specificity and the Dice similarity coefficient. It can be observed from Fig. 8a that the adaptive threshold in LCX segmentation leads to a reasonable score for all the accuracy metrics, whereas high false positives associated with the fixed threshold leads to low specificity and a decreased Dice coefficient score (see Fig. 8b for the fixed threshold). Similarly, the use of adaptive threshold results in a stable value for all three metrics in RCA segmentation (Fig. 8c), whereas the fixed threshold leads to increased false negatives causing a significant drop in the sensitivity and the corresponding Dice similarity coefficient (Fig. 8d). Moreover, the mean Dice similarity for two segmentation methods is presented in Fig. 2b which clearly demonstrates the efficacy of adaptive threshold over fixed intensity threshold (specifically for volumes with irregular concentration of dye i.e. volume 1, 6, 7, 8 and 11).

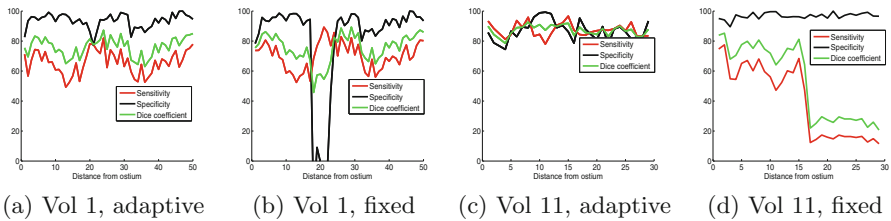


Fig. 8. Segmentation accuracy for fixed and the adaptive threshold based segmentation. (a–b) Results for LCX segment of CTA volume 1 where high false positives lead to low specificity and decreased Dice score, (c–d) results for RCA segment of CTA volume 11 where high false negatives lead to low sensitivity and decreased Dice score.

4 Conclusion

We demonstrated that adaptive modelling of the contrast medium intensity can considerably improve the accuracy of the coronary segmentation. In contrast, the use of a fixed intensity threshold across the dataset may decrease precision by capturing the nearby non-coronary segments or missing the distal parts of coronary tree. After deriving the volume-specific intensity ranges, we employed a bi-directional level set based Chan-Vese evolution to segment the coronary tree from CTA volume. Promising results validating a significant improvement in segmentation quality confirms the need of contrast medium modelling in segmentation process. A limitation of the current method is its failure to detect non-calcified plaques which exhibit an unexpected intensity drop across the lesion regions of the coronary tree, which is being investigated in an ongoing study.

References

1. Caselles, V., Kimmel, R., Sapiro, G.: Geodesic active contours. *Int. J. Comput. Vis.* **22**(1), 61–79 (1997)

2. Chan, T.F., Vese, L.A.: Active contours without edges. *IEEE Trans. Image Process.* **10**(2), 266–277 (2001)
3. Dodge, J.T., Brown, B.G., Bolson, E.L., Dodge, H.T.: Lumen diameter of normal human coronary arteries. influence of age, sex, anatomic variation, and left ventricular hypertrophy or dilation. *Circulation* **86**(1), 232–246 (1992)
4. Duda, R.O., Hart, P.E.: Use of the hough transformation to detect lines and curves in pictures. *Commun. ACM* **15**(1), 11–15 (1972)
5. Frangi, A.F., Niessen, W.J., Vincken, K.L., Viergever, M.A.: Multiscale vessel enhancement filtering. In: Wells, W.M., Colchester, A., Delp, S. (eds.) *MICCAI 1998*. LNCS, vol. 1496, pp. 130–137. Springer, Heidelberg (1998). doi:[10.1007/BFb0056195](https://doi.org/10.1007/BFb0056195)
6. Hernandez, M., Frangi, A.F., Sapiro, G.: Three-dimensional segmentation of brain aneurysms in CTA using non-parametric region-based information and implicit deformable models: method and evaluation. In: Ellis, R.E., Peters, T.M. (eds.) *MICCAI 2003*. LNCS, vol. 2879, pp. 594–602. Springer, Heidelberg (2003). doi:[10.1007/978-3-540-39903-2.73](https://doi.org/10.1007/978-3-540-39903-2.73)
7. Hong, C., Becker, C.R., Schoepf, U.J.: Coronary artery calcium: absolute quantification in nonenhanced and contrast-enhanced multi-detector row ct studies 1. *Radiology* **223**(2), 474–480 (2002)
8. Isgum, I., van Ginneken, B., Olree, M.: Automatic detection of calcifications in the aorta from CT scans of the abdomen 1: 3D computer-aided diagnosis. *Acad. Radiol.* **11**(3), 247–257 (2004)
9. Kass, M., Witkin, A., Terzopoulos, D.: Snakes: active contour models. *Int. J. Comput. Vis.* **1**(4), 321–331 (1988)
10. Lankton, S., Tannenbaum, A.: Localizing region-based active contours. *IEEE Trans. Image Process.* **17**(11), 2029–2039 (2008)
11. Li, C., Kao, C.Y., Gore, J.C., Ding, Z.: Implicit active contours driven by local binary fitting energy. In: *IEEE Conference on Computer Vision and Pattern Recognition*, pp. 1–7. IEEE (2007)
12. Mohr, B., Masood, S., Plakas, C.: Accurate lumen segmentation and stenosis detection and quantification in coronary CTA. In: *Proceedings of 3D Cardiovascular Imaging: A MICCAI Segmentation Challenge Workshop* (2012)
13. NHS, UK: Coronary Heart Disease, Statistics for United Kingdom. <http://www.nhs.uk/Conditions/Coronary-heart-disease/Pages/Introduction.aspx>. Accessed 11 Nov 2016
14. Sethian, J.A., et al.: Level set methods and fast marching methods. *J. Comput. Inf. Technol.* **11**(1), 1–2 (2003)
15. Szymczak, A., Stillman, A., Tannenbaum, A., Mischaikow, K.: Coronary vessel trees from 3D imagery: a topological approach. *Med. Image Anal.* **10**(4), 548–559 (2006)
16. Van Uitert, R., Bitter, I.: Subvoxel precise skeletons of volumetric data based on fast marching methods. *Med. Phys.* **34**(2), 627–638 (2007)
17. Wang, Y., Liatsis, P.: A fully automated framework for segmentation and stenosis quantification of coronary arteries in 3D CTA imaging. In: *DESE 2009*, pp. 136–140. IEEE (2009)
18. Yang, Y.: Image segmentation and shape analysis of blood vessels with applications to coronary atherosclerosis. Ph.D. thesis, Georgia Institute of Technology (2007)
19. Yezzi, A., Tsai, A., Willsky, A.: A fully global approach to image segmentation via coupled curve evolution equations. *J. Vis. Commun. Image Represent.* **13**(1), 195–216 (2002)